SUPPORTING INFORMATION

Self-encapsulating Ag nanospheres in amorphous carbon: A novel ultrathin selective absorber for flexible solar-thermal conversion

Wei Li,[a] Chengbing Wang,[a,b,*] Jinzhu Yang,[a] Jiulong Wang,[a] Wenhe Zhang[a]

[a] College of Materials Science and Engineering, Shaanxi Key Laboratory of Green Preparation and Functionalization for Inorganic Materials, Shaanxi University of Science and Technology, Xi'an, 710021, P. R. China

[b] Zhejiang Wenzhou Research Institute of Light Industry, Wenzhou 325003, Zhejiang, China.

[*]Address Correspondence to wangchengbing@gmail.com

Corresponding theoretical calculation formula

(1) Optical absorption (α):

$$\alpha = \int_{200nm}^{2500nm} \frac{I_s(\lambda)(1 - R(\lambda))d\lambda}{I_s(\lambda)d\lambda}$$

(2) Infrared thermal emissivity (ε):

$$\varepsilon = \int_{2.5\mu m}^{25\mu m} \frac{I_b(\lambda,T)(1 - R(\lambda))d\lambda}{I_b(\lambda,T)d\lambda}$$

$$I_b(\lambda,T) = \frac{C_1}{\lambda^5 \times \left[e^{C_2/(\lambda T)} - 1\right]}$$

Where λ is wavelength, R(λ) is measured reflection spectrum, $I_s(\lambda)$ is 1.5AM Spectral irradiation, $I_b(\lambda,T)$ represents black body radiation, where $C_1 = 3.743 \times 10^{-16} Wm^2$, $C_2 = 1.4387 \times 10^{-2}$ mK

(3) photothermal conversion efficiency (η):

$$\eta = \alpha - \frac{\sigma T^4}{CQ_1}\varepsilon$$

Where σ , T, C, Q_1 are Stefan-Boltzmann constant (5.67×10^{-8} W/m^{2}K^4), working temperature (353.15K), solar concentration factor (1 sun), solar flux intensity(1kW/m^2), respectively.

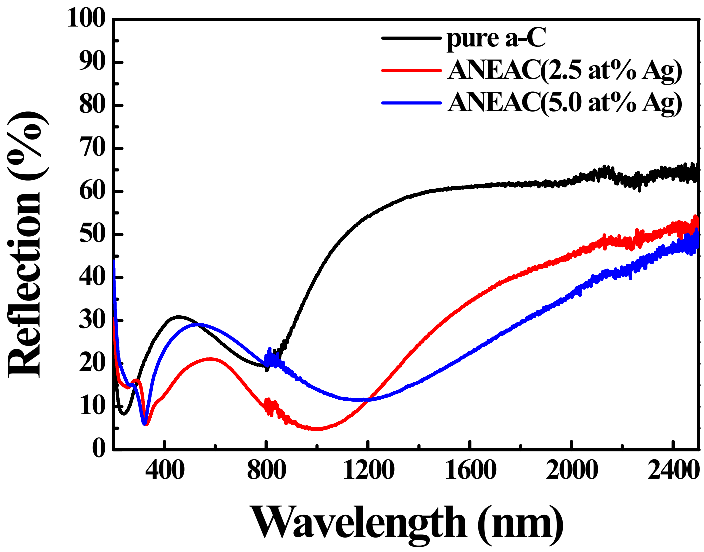

Fig. S1. The reflectance spectrum of ANEAC film with different Ag doping content between 200 nm to 2500 nm.

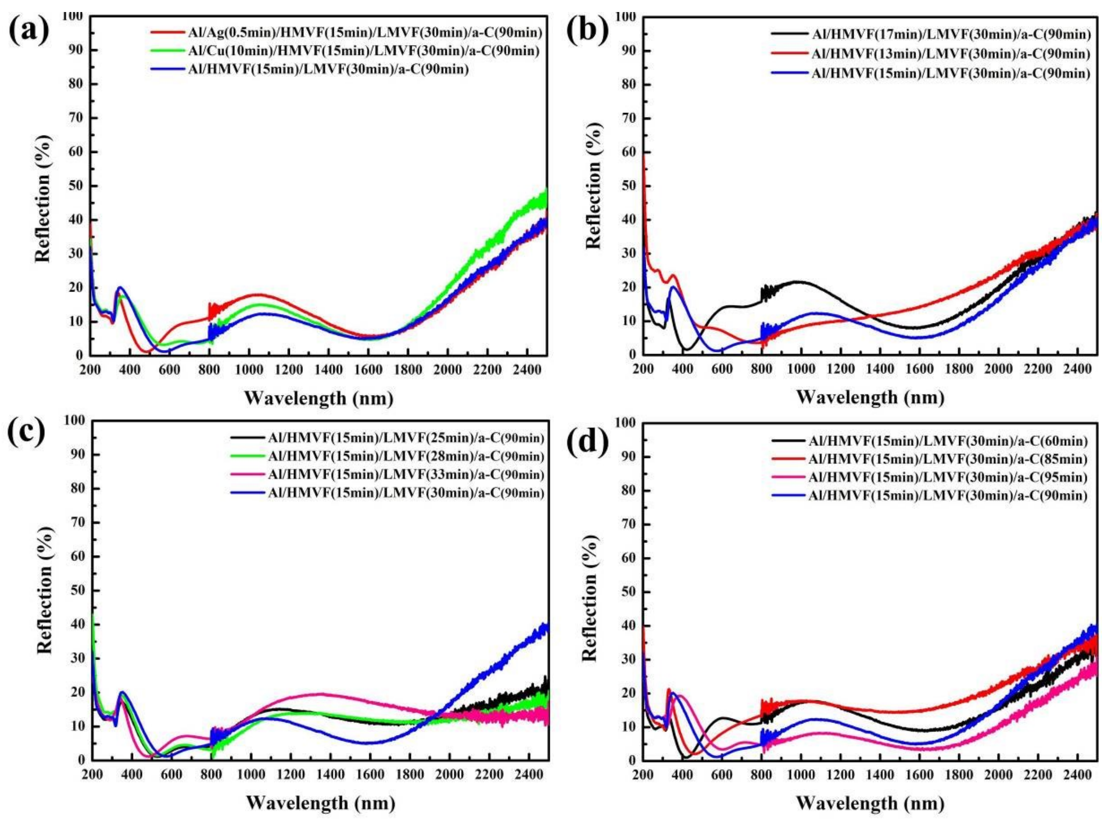

Fig. S2. Influence of single-layer deposition time (thickness) on the absorption of SSAs (Taking the sample (Al/HMVF (15 min)/LMVF (30 min)/a–C (90 min) as reference). (a) The change of coating reflectivity before and after adding (Ag or Cu) infrared-reflective layer. (b–d) The variety curve of coating reflectivity with different deposition times of HMVF layer, LMVF layer, and a–C layer, respectively.

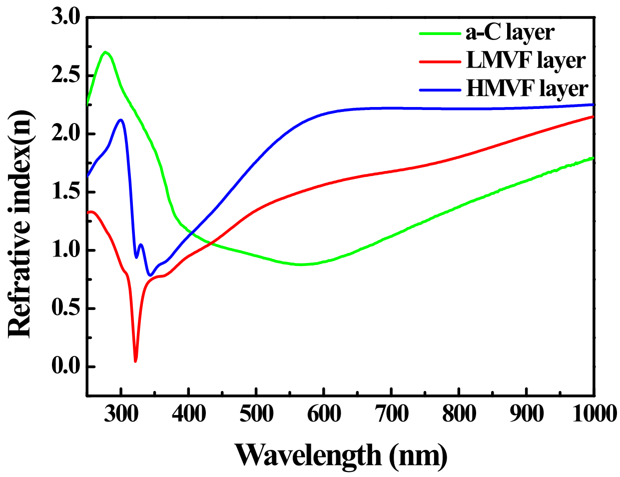

Fig. S3. The refractive index change curve of a-C layer, HMVF layer and LMVF layer.

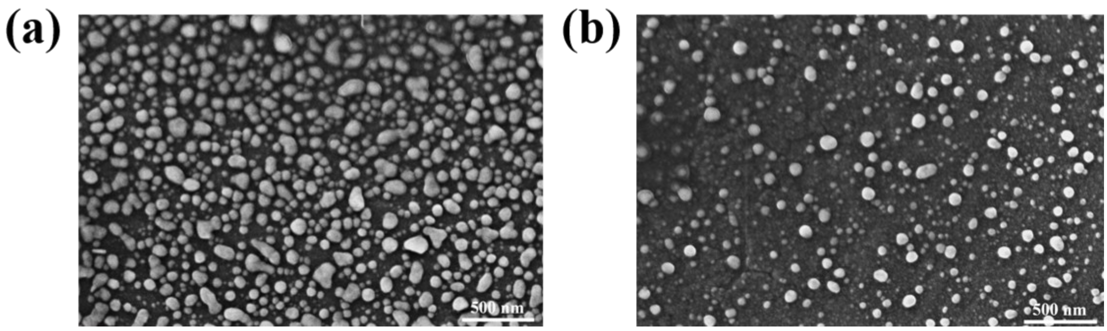

Fig. S4. Scanning image of ANEAC surface with different silver content: (a) HMVF layer; (b) LMVF layer.

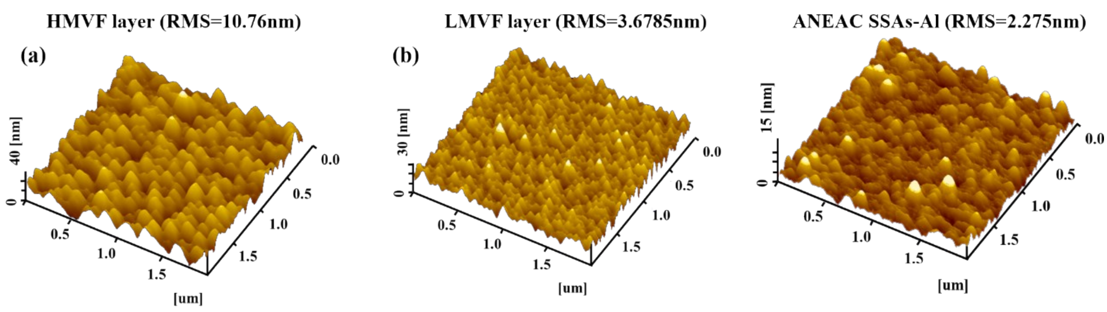

Fig. S5. Variation of surface roughness with different Ag content: (a) HMVF layer; (b) LMVF layer; c) Al/HMVF/LMVF/a–C SSAs.

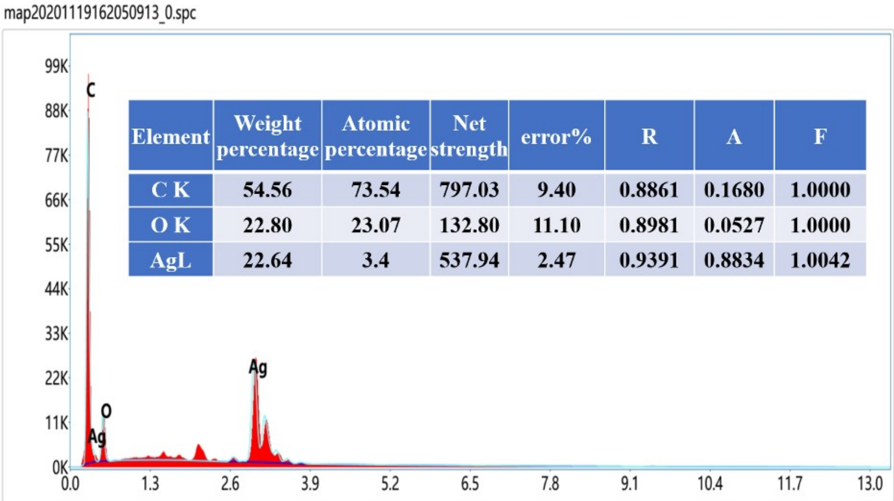

Element	Weight percentage	Atomic percentage	Net strength	error%	R	A	F
C K	54.56	73.54	797.03	9.40	0.8861	0.1680	1.0000
O K	22.80	23.07	132.80	11.10	0.8981	0.0527	1.0000
AgL	22.64	3.4	537.94	2.47	0.9391	0.8834	1.0042

Fig. S6. Mapping of ANEAC SSAs–CT.

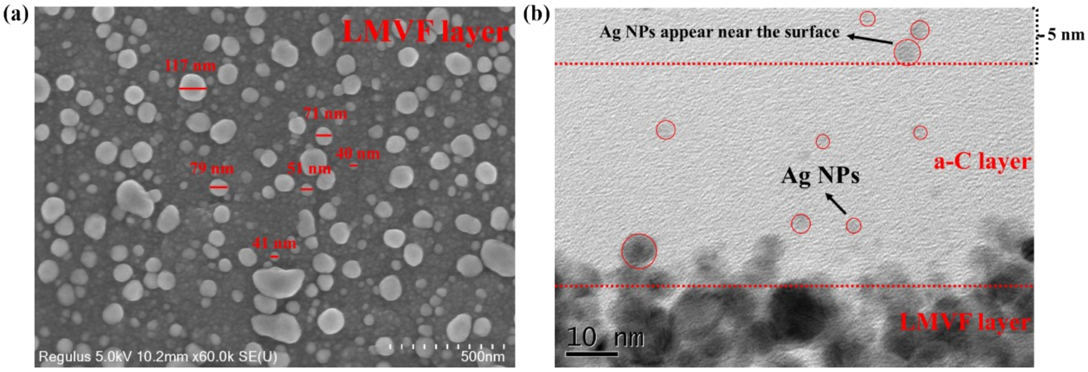

Fig. S7 (a) Surface topography of LMVF layer; (b) Cross-sectional TEM image of a-C layer.

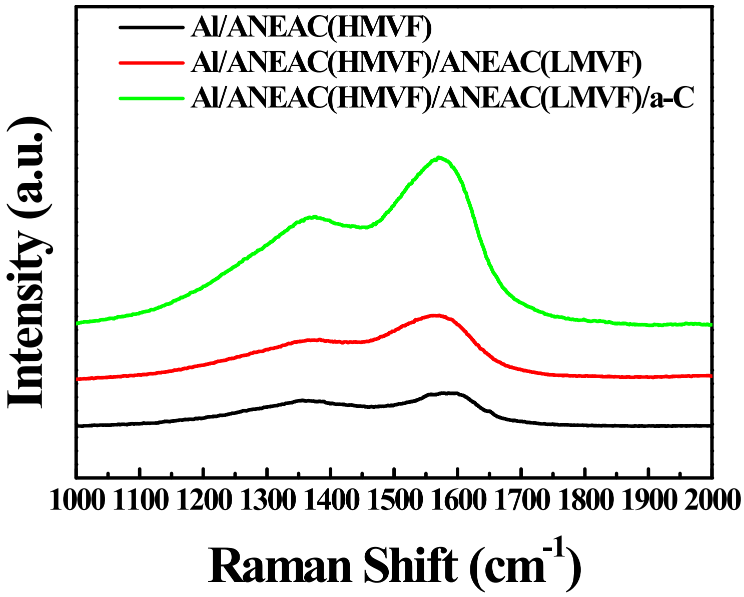

Fig. S8. Raman spectrum of layer-added of ANEAC SSAs–Al.

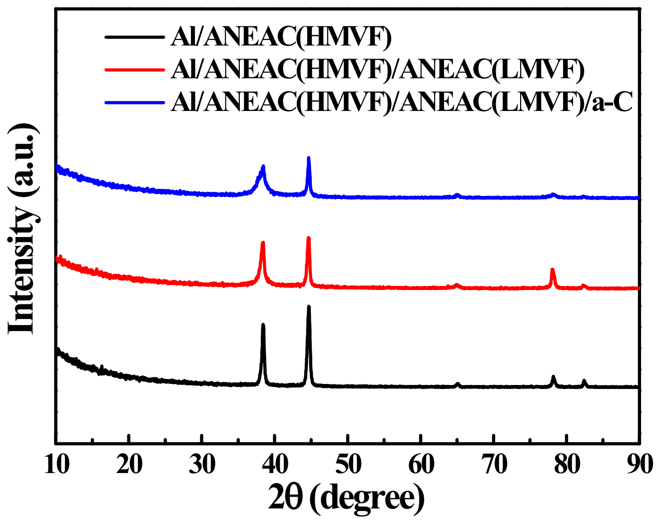

Fig. S9. XRD spectrum of layer-added of ANEAC SSAs–Al.

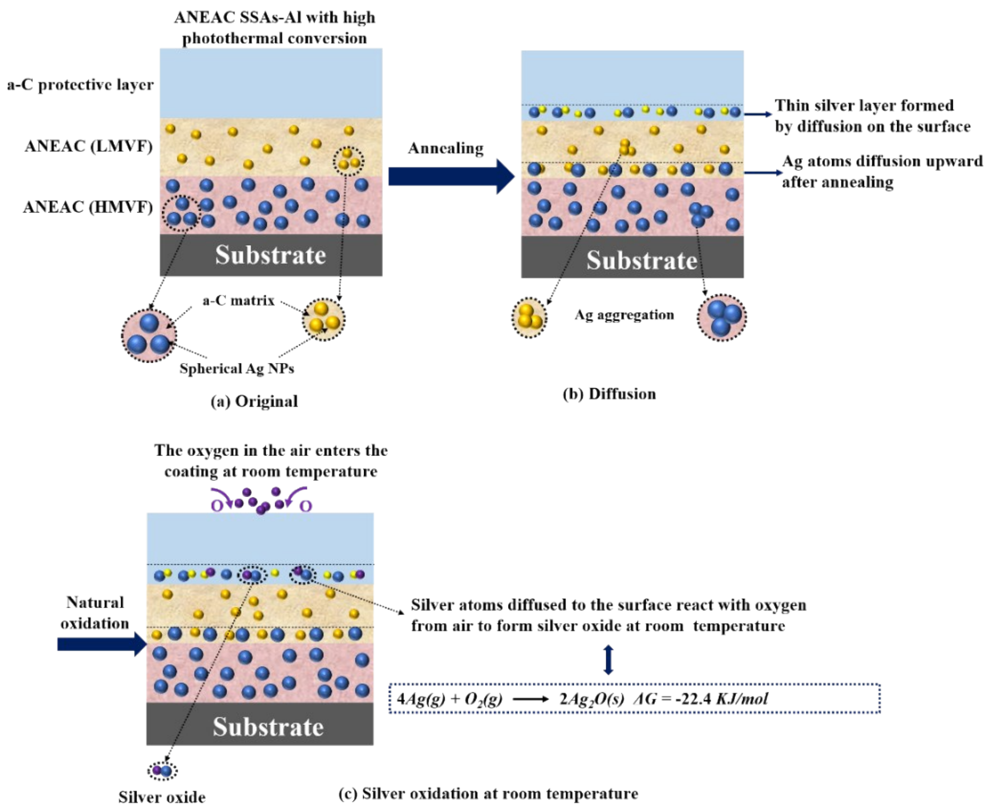

Fig. S10. Thermal stability mechanism of ANEAC SSAs–Al.

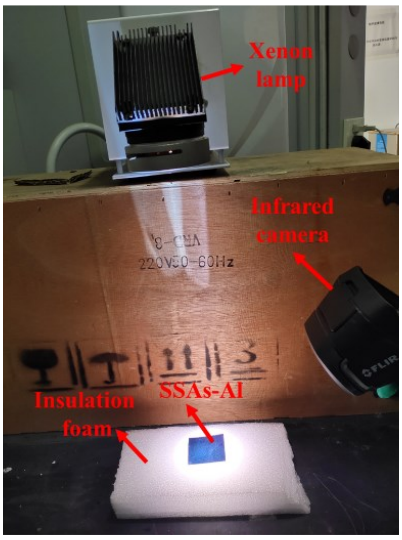

Fig. S11. The device diagram of photothermal experiment for ANEAC SSAs under standard solar radiation.

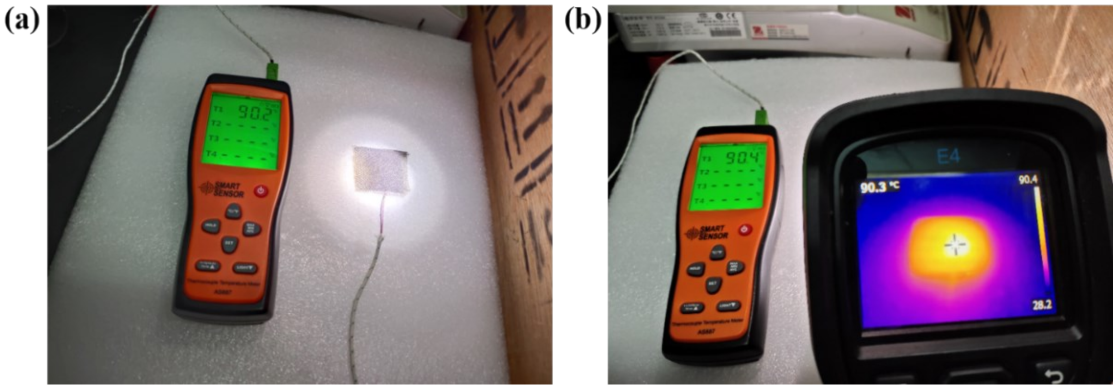

Fig. S12. (a) Using thermocouple alone to measure the temperature of SSAs-CT;(b) Use thermocouple and infrared camera to measure the temperature of SSAs-CT simultaneously.

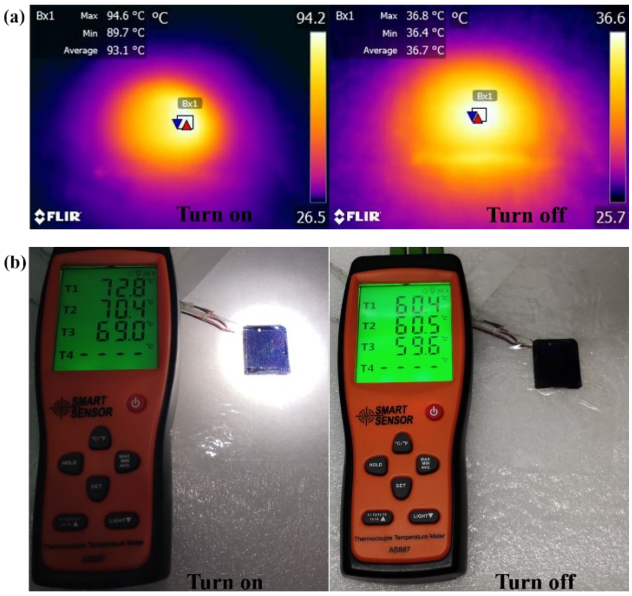

Fig. S13. (a) Using an infrared camera to measure the average surface temperature of the SSAs-CT before and after turning off the lights; (b) Using a thermocouple to measure the average temperature of the SSA-Al surface before and after turning off the light (Measure the temperature at three different locations and take the average value)

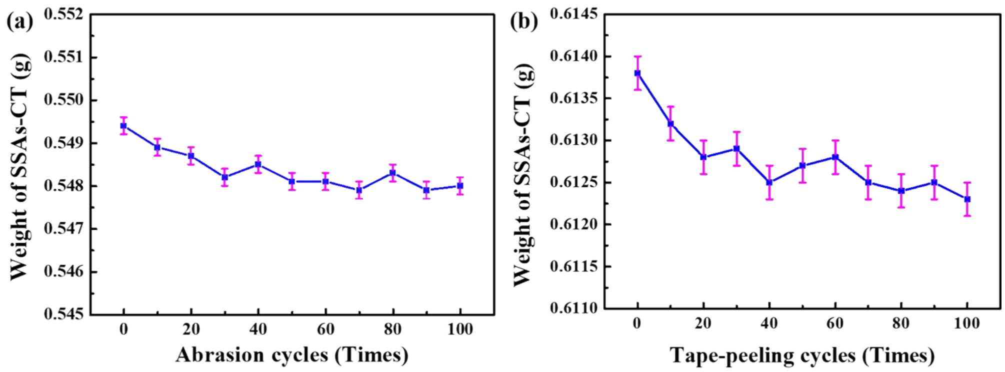

Fig. S14. The weight changes of ANEAC SSAs–CT before and after (a) abrasion cycles and (b) tape-peeling cycles.

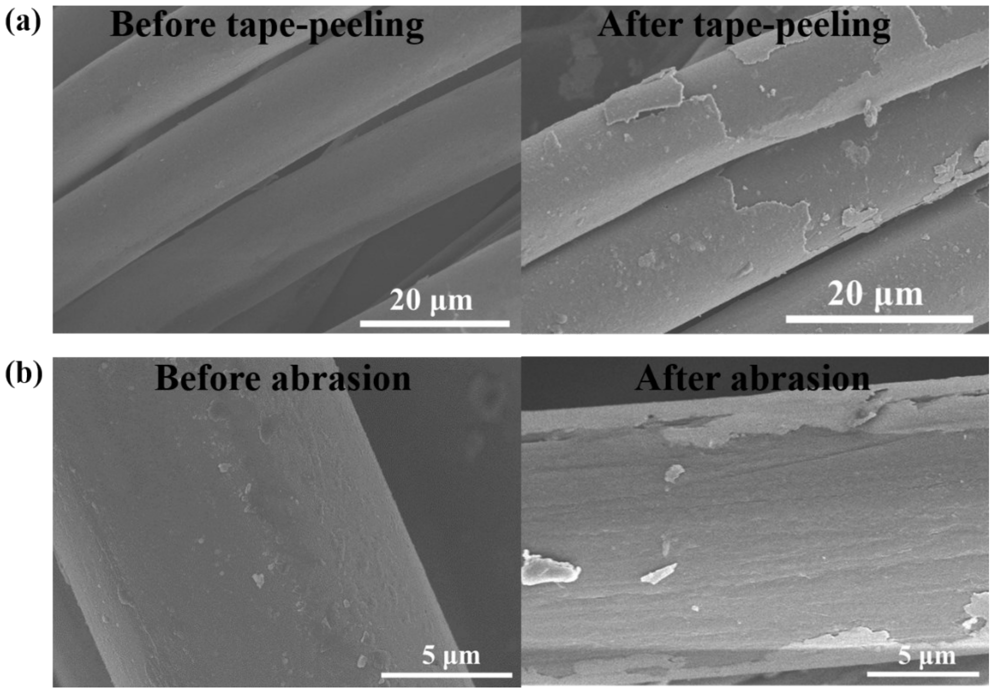

Fig. S15. Surface topography of ANEAC SSAs–CT before and after (a) tape-peeling and (b) abrasion cycles.

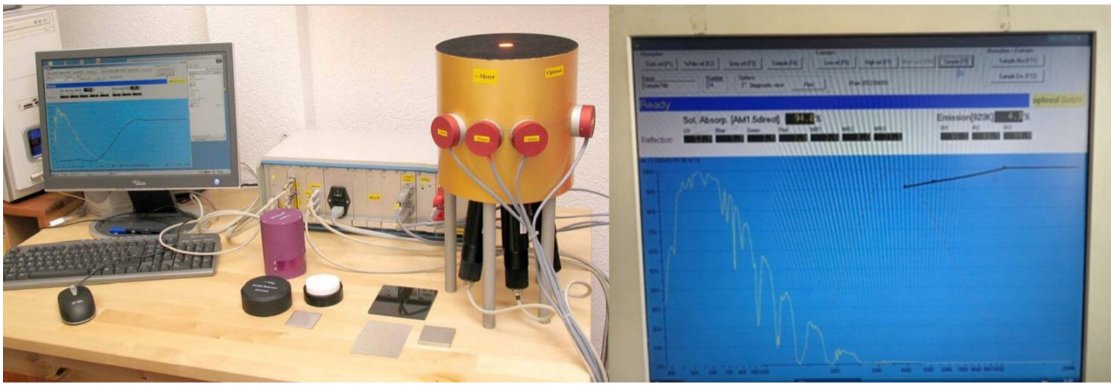

Fig. S16. The device and interface for K3 emissometer.

Table S1 Preparation parameters of ANEAC SSAs by co-sputtering.

Layer	RF power (W)	Cathode current (A)	Cathode voltage (V)	Deposition time (min)	Monolayer thickness (nm)
HMVF	200	0.02	230	15	40
LMVF	200	0.01	223	30	36
a–C	200	0	0	90	50

Table S2 Changes in absorptivity and thermal emissivity of ANEAC SSAs–Al with increasing annealing time.

Annealing time (h)	**α**	**ε**	**α/ε**
0	0.923	0.061	15.13
50	0.915	0.059	15.50
100	0.912	0.062	14.71
150	0.908	0.063	14.41
200	0.901	0.064	14.1

Table S3 Surface temperature of various photothermal materials under different solar radiation.

Solar absorber	Substrate	Surface temperature (ºC)	Irradiation intensity (kW/m^2)	Reference
Polydopamine (PDA)@Mxene	–	80	1	[34]
MXene/AgNW–PVA film	–	40.2	1	[35]
MXene–PVDF membrane	–	75	1	[36]
Graphene metamaterial	Cu foil	80	1	[37]
rGO–MWCNT/PVDF	–	77.6	1	[38]
Hydroxyapatite nanowires (HN)/CNT	paper	80	1	[39]
Single-walled carbon nanotube (SWCNT) film	–	76	1	[40]
CNT	Cotton cloth	82.4	1	[41]
MWCNTs@PPS/FC	paper	78	1	[42]
Ti/MgF_2/CT	Cu mesh	60	1	[43]
W/W–WO_x (HA)/W–WO_x (HA)/WO_x	PI sheet	78.1	1	[44]
Mo/Mo–MoO_x (HA)/ Mo–MoO_x (HA)/MoOx	Cotton cloth	90	1	[45]
Bilayer single-walled carbon nanotube/AuNR film	–	95	5	[46]
CuS/polyethylene (PE) hybrid membrane	–	52	1	[47]
Flexible Ti_2O_3–PVA nanocomposite film	–	64.1	5	[48]